

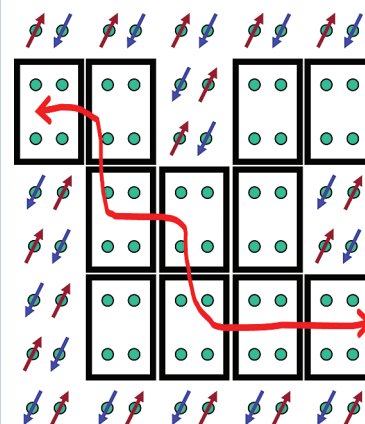
Universal Properties of Cuprate Superconductors: T_c Phase Diagram, Room-Temperature Thermopower, Neutron Spin Resonance, and STM Incommensurability Explained in Terms of Chiral Plaquette Pairing

Jamil Tahir-Kheli* and William A. Goddard III*

Materials and Process Simulation Center (MC 139-74), California Institute of Technology, Pasadena, California 91125

ABSTRACT We report that four properties of cuprates and their evolution with doping are consequences of simply counting four-site plaquettes arising from doping. (1) the universal T_c phase diagram (superconductivity between ~ 0.05 and ~ 0.27 doping per CuO_2 plane and optimal T_c at ~ 0.16), (2) the universal doping dependence of the room-temperature thermopower, (3) the superconducting neutron spin resonance peak (the “41 meV peak”), and (4) the dispersionless scanning tunneling conductance incommensurability. Properties (1), (3), and (4) are explained with no adjustable parameters, and (2) is explained with exactly one. The successful quantitative interpretation of four very distinct aspects of cuprate phenomenology by a simple counting rule provides strong evidence for four-site plaquette percolation in these materials. This suggests that inhomogeneity, percolation, and plaquettes play an essential role in cuprates. This geometric analysis may provide a useful guide to search for new compositions and structures with improved superconducting properties.

SECTION Electron Transport, Optical and Electronic Devices, Hard Matter



We provide a simple explanation of the universal dependence of four properties of cuprate superconductors on doping (x) in the CuO_2 planes: (1) the universal dependence of T_c (superconductivity between $x \approx 0.05$ and 0.27 doping per CuO_2 plane and optimal T_c at ~ 0.16),^{1,2} (2) the room-temperature thermopower (Seebeck effect),^{1–5} (3) the neutron spin (π, π, π) resonance peak,^{6–22} and (4) the nondispersing conductance incommensurabilities in STM (observed thus far only for single-layer Bi-2201).^{23,24}

It is hard to imagine four experiments that are more different. The T_c phase diagram is due to the nature of the superconducting pairing and its doping evolution, the universal thermopower is observed in the normal state near room temperature and relates simultaneous heat and charge transport, the neutron resonance probes spin fluctuations, and the STM measures local density of states (LDOS) variations on an atomic scale. We explain all four experiments here using simple counting arguments.

It is well-known that the superconducting critical temperature, T_c , for all cuprates fits the expression $(T_c/T_{c,\text{max}}) \approx 1 - 82.6(x - 0.16)^2$, where x is the hole doping per Cu in the CuO_2 planes.^{1,2} This leads to the three universal doping values, where superconductivity first appears at $x \approx 0.05$, is optimal at $x \approx 0.16$, and disappears above $x \approx 0.27$. This remarkable universality has not been explained.

The room-temperature (290 K) thermopower, or Seebeck effect, for all cuprates decreases strongly with increased doping (from +80 to $-13 \mu\text{V/K}$) with the same universal

dependence. In addition, the temperature dependence at high temperatures is anomalous. Rather than $S = BT$, as expected from entropy transport due to electrons in metals (the Mott formula), all cuprates have the form $A + BT$, where A is large and strongly doping-dependent while B is doping-independent.^{1–5}

The neutron spin inelastic scattering shows a very strong resonance near “41 meV” at the AF wavevector (π, π) [(π, π, π) in bilayer materials] that is nearly the same for all cuprates, but doping-dependent while tracking T_c .^{25,26} The peak occurs at the center of an “hourglass” dispersion with the high energy sheet doping-independent and the lower sheet doping- and material-dependent.^{27–30}

The recently observed doping-dependent STM incommensurability in single-layer Bi-2201^{23,24} is anomalous because the wavelength increases with increasing doping rather than decreasing with increasing doping, as expected from the mean separation of holes.

No theory has yet explained all four within a single framework. Electronic and small polaron models have been proposed for the T_c phase diagram^{31–33} and spin-vortex and stripe models for the neutron resonance.^{21,34,35} We show here that simple counting combined with a few simple assumptions

Received Date: February 24, 2010

Accepted Date: March 26, 2010

Published on Web Date: April 01, 2010

regarding the character of the doping quantitatively explains the thermopower with exactly one adjustable parameter while simultaneously explaining the other three experiments with no adjustable parameters. Our assumptions are derived from the results of ab initio B3LYP DFT calculations on undoped and explicitly doped $\text{La}_{2-x}\text{Sr}_x\text{CuO}_4$ ^{36,37} and our chiral plaquette pairing model (CPP).^{38,39}

Our model for doping rests on three assumptions. First, doping leads to a hole in an out-of-the-plane impurity orbital with $\text{O p}_z\text{-Cu d}_{z^2}\text{-O p}_z$ character that is orthogonal to the planar $\text{Cu/O } x^2-y^2/p\sigma$ band. Our QM calculations³⁶⁻³⁹ show that this orbital is delocalized over a four-site square Cu plaquette in the vicinity of the dopant and is comprised (for LSCO) predominantly of apical O p_z (above Cu in CuO_2 plane) and Cu d_{z^2} hole character. We refer to the four Cu sites included in the four-site plaquettes as doped sites. The undoped Cu sites remain localized d^9 states with neighboring AF coupling $J_{dd} = 0.13 \text{ eV} = 130 \text{ meV}$ (the value found in undoped materials^{40,41}). Figure 1 shows a 2D snapshot at doping $x = 0.16$.

We assume that placing dopants on neighboring sites leads to repulsive interaction, so that there are no plaquette overlaps. For the calculations in this paper, we assume a more restrictive doping for which the plaquette centers are always separated by an even number of Cu-Cu lattice spacings, as shown in Figure 1. This allows doping up to $x = 0.25$ with no plaquette overlap and leads to analytic expressions for the quantities of interest. This restriction does not alter the results in this paper (see Supporting Information).

Second, as doping increases, there is a critical concentration above which the four-site plaquettes percolate through the crystal. In this regime, we expect that the planar $\text{Cu/O } x^2-y^2/p\sigma$ orbitals on the doped sites inside of the percolating swath delocalize to form the standard $\text{Cu/O } x^2-y^2/p\sigma$ metallic band. This is because the $\text{Cu } x^2-y^2$ orbital energy is lowered relative to the $\text{O p}\sigma$ due to the reduced Coulomb repulsion from the hole in the out-of-the-plane plaquette state. This increases the effective Cu-Cu hopping relative to the undoped sites and leads to delocalization, as shown in Figure 2.

These two assumptions lead to three types of electrons, (1) the undoped Cu d^9 spins (dots in Figure 1) that are coupled to each other with the undoped AF $J_{dd} = 130 \text{ meV}$, (2) the $\text{Cu/O } x^2-y^2/p\sigma$ metallic band inside of the percolating plaquette region (inside squares in Figure 1), and (3) the hole comprising the four-site plaquette orbital that is orthogonal to the $\text{Cu/O } x^2-y^2/p\sigma$ metallic band (shown as squares in Figure 1). Figure 1 also distinguishes surface plaquettes in contact with undoped d^9 spins (red squares) and interior plaquettes not in contact with d^9 spins (blue squares).

Third, we assume that superconducting pairing occurs only for surface plaquettes (adjacent to undoped d^9 sites). We argued previously^{38,39} that this occurs because the interaction with the d^9 spins makes these plaquettes chiral, but such detail is not necessary for the results presented here.

On the basis of the above assumptions, the onset of superconductivity occurs when the four-site plaquettes percolate in three dimensions (3D) because a metallic band is formed on the percolating swath. Using a linear algorithm,⁴² we calculate that 3D percolation occurs at $x = 0.066$ holes per CuO_2 plane (experimental value 0.053 ⁴³). Similar calculations

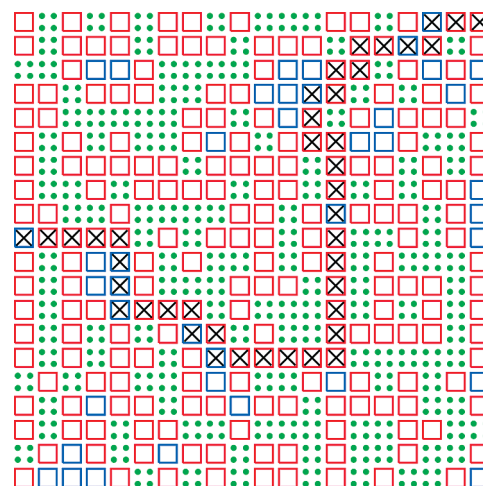


Figure 1. (a) Illustration of the three types of electrons in a single CuO_2 plane for $x = 0.16$ doping. Green dots indicate undoped Cu d^9 spins that are AF coupled. Each square indicates a four-site plaquette centered at a dopant and comprised of out-of-plane orbitals (apical O p_z and Cu d_{z^2}). The dopants are distributed randomly within the condition of even separations. The red (blue) squares are surface (interior) plaquettes. A $\text{Cu/O } x^2-y^2/p\sigma$ metallic band forms inside of the percolating region of the plaquettes due to $\text{Cu } x^2-y^2$ orbital energy lowering relative to $\text{O p}\sigma$, as shown in Figure 2. The crosses schematically show one percolating path. Optimal doping, $x = 0.16$, is shown.

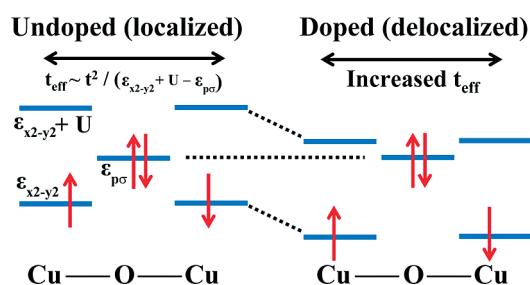


Figure 2. Localized hole formation in out-of-the-plane Cu d_{z^2} and apical O p_z orbitals leads to delocalization of the Cu d^9 spins within the plaquette swath due to increased Cu-Cu hopping in the CuO_2 plane arising from the stabilization of the $\text{Cu d}_{x^2-y^2}$ orbital energy relative to the planar $\text{O p}\sigma$. In the undoped regions, localized Cu d^9 spins remain.

assuming a staggered CuO_2 planar structure in $\text{La}_{2-x}\text{Sr}_x\text{CuO}_4$ lead to ~ 0.05 .

It has recently been shown in LSCO ⁴³ that the T_c at the transition to superconductivity does not start at $T_c = 0$ but instead jumps to a finite value of $\sim 3.5 \text{ K}$. In our model, the number of superconducting electrons is $4x$, and the strength of the pairing is proportional to the number of surface plaquettes. Thus, at the point at which percolation is achieved, $x = 0.053$, the strength of the pairing should be proportional to $4x = 0.2$, leading to a jump to finite T_c at the transition, consistent with experiment.

At doping, $x = 0.25$, our model implies that no undoped Cu d^9 sites are left to induce superconducting pairing. This leads to $x = 0.25$ as the maximum doping for superconductivity (experimental value ≈ 0.27). See Supporting Information for further details.

The optimal T_c occurs when the pairing maximizes the energy lowering. This occurs when the number of electrons that can pair [the density of states at the Fermi level, $N(0)$] times the pairing energy, V , is maximized. Thus optimal T_c occurs when $N(0)V$ is maximized.

In our model, $N(0) \approx \Omega_M/\Omega_{\text{total}}$, where Ω_M is the number of metallic sites (doped Cu sites) and Ω_{total} is the total number of sites. $\Omega_M/\Omega_{\text{total}} = 4x$ since each plaquette adds four Cu sites to the metallic swath. The pairing strength is the ratio of the number of surface plaquettes, S_p , to the number of metallic sites, $V \approx S_p/\Omega_M$, leading to $N(0)V \approx S_p/\Omega_{\text{total}}$.

With random doping, the probability that a plaquette is surrounded by four plaquettes is $(4x)^4$. The probability that the plaquette is on the surface (has at least one AF d^9 neighbor) is $1 - (4x)^4$, leading to $S_p/\Omega_{\text{total}} = x[1 - (4x)^4]$. The maximum occurs at $x = 1280^{-1/4} \approx 0.167$ (experimental value ≈ 0.16). The optimal doping value does not depend on differences of the Cooper pairing temperature, T_p , and the pair phase coherence temperature, T_ϕ , because, generally, $T_c = \min(T_p, T_\phi)$, and optimal doping occurs at the crossover from the phase fluctuation to pairing regime, $T_p = T_\phi$.⁴⁴ This explains the three universal doping values of the superconducting phase.

The undoped d^9 clusters in Figure 1 (green dots) are described by the Heisenberg AF spin Hamiltonian with the undoped AF coupling, $J_{dd} = 130$ meV. These finite AF clusters will spin-couple to neighboring AF clusters through the metallic $x^2-y^2/p\sigma$ electrons and by coupling with the surface plaquette hole spins. The random locations of the surface plaquettes lead to a disordered magnet with a finite spin correlation length, ξ . The (π, π) state [or the (π, π, π) state in bilayer systems] has zero excitation energy in the infinite 2D Heisenberg antiferromagnet, but will be gapped due to the disorder. We estimate the excitation energy, E_{res} , by $E_{\text{res}} = \hbar c_{\text{sw}}/2\xi$, where c_{sw} is the undoped AF magnon spin velocity. This is derived by applying the uncertainty principle, $\Delta x \Delta p = \hbar/2$, to the spin-wave dispersion, $\hbar\omega = c_{\text{sw}}\Delta p$, and choosing $\Delta p = \hbar/2\xi$.

The spin-wave velocity, c_{sw} , is determined from the undoped AF coupling, J_{dd} , and harmonic spin-wave expansions,⁴⁵ $\hbar c_{\text{sw}} = 2^{1/2}Z_c J_{dd} a$, where a is the Cu–Cu lattice distance and $Z_c \approx 1.18$. The correlation length, ξ , is the mean spacing between surface plaquettes, $\xi = (S_p/\Omega_{\text{total}})^{-1/2} a$, and is known as a function of doping, x , as shown above, while x can be obtained from the universal doping $T_c/T_{c,\text{max}}$ equation,^{1,2} as described above. Thus, the neutron resonance energy, E_{res} , is completely determined with no adjustable parameters. Since ξ is shortest at optimal T_c , the resonance peak tracks T_c rather than increasing for increasing doping away from the undoped AF phase.^{25,26}

Table 1 compares our calculated resonance peak energy with experiment for underdoped, optimally doped, and overdoped cuprates YBCO, Bi-2212, and Tl-2201. The fit is very good.

The energy-integrated neutron peak susceptibility, $\int d\omega \chi''(q, \omega)$, where $q = (\pi, \pi, \pi)$, is known experimentally and can be estimated by summing the contribution to the integral from each finite cluster. This estimate is reasonable since the correlation length is on the order of the cluster sizes.

Table 1. Calculated Neutron Resonance Peak Energy versus Experiment for Under-, Optimal, and Overdoped (UD, OP, OD) Bi-2212, YBCO, and Tl-2201^a

material	T_c (K)	doping (x)	S_p/Ω_{tot}	resonance energy (meV)	
				experiment	theory
YBCO _{6.5} (UD)	52	0.087	0.086	25	31.7
YBCO _{6.7} (UD)	67	0.102	0.099	33	34.1
YBCO _{6.9} (OP)	93	0.167	0.133	41	39.6
Tl-2201 (OP)	90	0.167	0.133	47	39.6
Bi-2212 (OP)	91	0.167	0.133	43	39.6
Bi-2212 (OD)	87	0.183	0.130	42	39.1
Bi-2212 (OD)	83	0.193	0.124	38	38.2
Bi-2212 (OD)	70	0.213	0.101	34	34.4

^a The data is from refs 9, 10, and 15. We used $T_{c,\text{max}} = 93, 90$, and 91 K for YBCO, Tl-2201, and Bi-2212, respectively, to obtain the doping, x , in column 3 by applying $(T_c/T_{c,\text{max}}) \approx 1 - 82.6(x - 0.16)^2$. The number of surface plaquettes is given by $S_p/\Omega_{\text{tot}} = x[1 - (4x)^4]$. $E_{\text{res}} = \hbar c_{\text{sw}}/2\xi$, where $\xi = (S_p/\Omega_{\text{tot}})^{-1/2} a$ and $\hbar c_{\text{sw}} = 2^{1/2} Z_c J_{dd} a$, with $Z_c \approx 1.18$.⁴⁵

We computed the $S = 0$ ground state and $S = 1$ first excited state for all AF cluster shapes and sizes up to 24 spins (24 AF spins required Lanczos diagonalization over $\sim 2.7 \times 10^6$ states) along with the corresponding spin–flip matrix elements to obtain an energy-integrated spectral weight of $5.1\mu_B^2$ per f.u. for optimal doping (see Supporting Information). Experiment finds 1.9 for optimally doped Bi-2212 and 1.6 for YBCO.^{9,11} Our estimated result is approximately 2.5 times larger than experiment. Generally, models that attribute the resonance to Fermi surface effects are an order of magnitude smaller. A phenomenological (π, π) spin-fluctuation enhancement is invoked to scale the value up to experiment.

The experimental neutron resonance width, Γ , is found to be resolution-limited (~ 5 meV) in YBCO and slightly broader than resolution for Bi-2212 in the superconducting state.^{9,11,15} This peak is substantially broadened in the normal state. We have calculated Γ at 20 K and at T_c for optimally doped YBCO and Bi-2212 using angle-resolved photoemission (ARPES) band structures for Bi-2212^{15,46} with an STM gap of 41.5 eV and from tight-binding models for YBCO^{47–49} with an STM gap of 20.0 eV. For YBCO, we calculated $\Gamma = 1.3$ and 45.3 meV at 20 and 92 K, and for Bi-2212, we found $\Gamma = 0.1$ and 22.8 meV at 20 and 92 K (see Supporting Information for details). Our calculated peaks are resolution-limited in the superconducting phase and are substantially broadened in the normal state (factor of ~ 30). The peak width for Bi-2212 is observed to be slightly broader than instrument resolution.¹⁵ This may be due to spatial variation of the gap.

The wavelength of the STM is given by the expected size of the metallic region between d^9 sites. The expected number of doped plaquettes between two d^9 regions is $1/(1 - 4x)$ since $1 - 4x$ is the probability that a plaquette is undoped (d^9). This leads to a total wavelength of $[2/(1 - 4x)] + 1$ in units of the Cu–Cu lattice spacing, a , since each plaquette is 2×2 Cu sites, and one further step is needed to get back to a d^9 site. Since the incommensurability is structural, it should be independent of the voltage. Table 2 shows the good fit to experiment.^{23,24}

Table 2. Comparison of Calculated Conductance Incommensurability versus Data on Bi-2201^a

T_c (K)	doping (x)	incommensurability (λ/a)	
		experiment ^{23,24}	theory
25	0.100	4.5 ± 0.2	4.3
32	0.128	5.1 ± 0.2	5.1
35	0.160	6.2 ± 0.2	6.6

^a λ is the incommensurability, and a is the planar Cu–Cu separation. The theoretical expression is $2/(1 - 4x) + 1$.

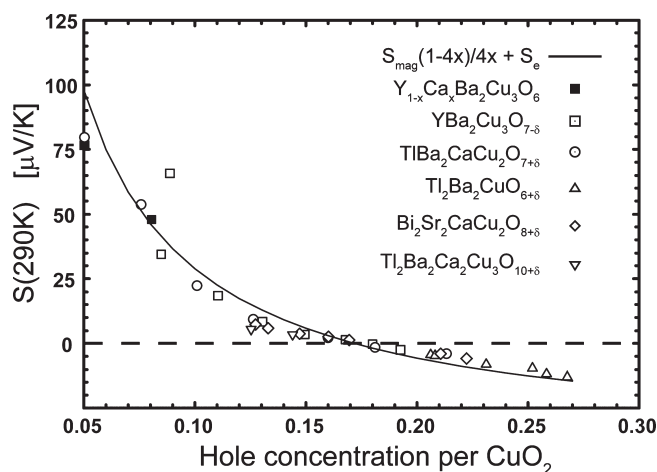


Figure 3. Fitting the thermopower at 290 K as a function of hole doping. The experimental data is from refs 1 and 2. The solid line is the prediction from the plaquette theory, $S(290\text{ K}) = S_{\text{mag}}(1 - 4x)/4x + S_e$, where $S_{\text{mag}} = 27.6\ \mu\text{V/K}$ and $S_e = -13\ \mu\text{V/K}$. S_{mag} is the only adjustable parameter.

An alternative explanation by Wise et al²³ is that this incommensurability arises from a charge density wave due to the Fermi surface nesting vector near $(\pi, 0)$ that decreases as hole doping increases.

Figure 3 shows that the universal room-temperature thermopower, $S(290\text{ K})$, decreases as a function of doping.^{1,2} The electronic thermopower, S_e , due to the $x^2 - y^2/p\sigma$ metallic electrons, leads to a linear temperature dependence with the magnitude depending on the derivative of the logarithm of the density states (DOS) and scattering time, τ (Mott formula^{50,51}). Any change in the DOS or τ by a constant factor due to doping does not change S_e . Thus, S_e at 290 K is doping-independent and cannot account for the observed doping-dependent room-temperature thermopower. Experiments in the nonsuperconducting region, $x > 0.27$, find $S_e \approx -13\ \mu\text{V/K}$.

Besides S_e , the plaquette model can lead to an additional contribution to the thermopower from the magnon drag arising from the nonequilibrium distribution of heat-carrying magnons in the undoped d^9 AF regions. By analogy to phonon drag,^{50–52} we expect that $S_{\text{mag}} = f(mc^2/e)(\tau_{\text{mag}}/\tau_e)(1/T)$, where m is the electron mass, e is the charge, c is the magnon spin-wave velocity, f is the fraction of $x^2 - y^2/p\sigma$ band momentum dissipated into magnons, τ_{mag} is the magnon scattering time, τ_e is the band scattering time, and T is temperature. At room temperature, $1/\tau_e \approx T$, and $f \approx S/\Omega_M$ is the ratio of the

surface area to the metallic swath. The magnons dissipate their momentum primarily by impurity scattering with the surface plaquettes and the metallic electrons. Thus, $1/\tau_{\text{mag}} \approx S/\Omega_{\text{AF}}$ is the ratio of the surface area of the d^9 regions to its size. This leads to $S_{\text{mag}} \approx \Omega_{\text{AF}}/\Omega_M = (1 - 4x)/4x$. The surface term and T cancel and lead to a constant.

Combining these terms, we get $S(290\text{ K}) = S_{\text{mag}}(1 - 4x)/4x + S_e$, where S_{mag} is an undetermined constant (best fit is $27.6\ \mu\text{V/K}$) and $S_e \approx -13\ \mu\text{V/K}$ from experiment.

Figure 3 shows the good fit of this expression for $x > 0.05$, where the metallic phase begins due to plaquette percolation.

In conclusion, we show that the simple assumption that dopants in cuprates lead to the formation of four-site plaquettes localized in the vicinity of the dopants with a $\text{Cu/O } x^2 - y^2/p\sigma$ metallic band created in the percolating region explains quantitatively the doping evolution of four universalities of cuprates. They are (1) the critical values for superconductivity (onset, optimal, and maximum doping), (2) the “41 meV” neutron spin resonance peak due to the finite correlation length of the AF regions between the percolating plaquette swaths, (3) the dispersionless STM incommensurability, and (4) the room-temperature thermopower due to magnon drag in the AF regions. The first three results are obtained with no adjustable parameters. The fourth is explained with exactly one adjustable parameter to fit experiment.

We believe the success in explaining four important, but seemingly unrelated, properties of the cuprates using only counting arguments is strong evidence for the role of four-site lattice plaquette percolation in cuprates. Since increasing the surface area to volume ratio increases T_c , we suggest that a higher T_c may be obtained by controlling the location of dopants.

SUPPORTING INFORMATION AVAILABLE Discussion of the general doping of plaquettes. Computational details of energy-integrated neutron susceptibility and spin resonance width. This material is available free of charge via the Internet at <http://pubs.acs.org>.

AUTHOR INFORMATION

Corresponding Author:

*To whom correspondence should be addressed. Fax: 626-585-0918. Tel: 626-395-8148. E-mail: jamil@wag.caltech.edu (J.T.-K.); wag@wag.caltech.edu (W.A.G.).

ACKNOWLEDGMENT The authors acknowledge discussions with V. Hinkov. Support for this research was provided by DOD-DARPA (0211720) and ONR-PROM (N00014-06-1-0938). The computational facilities at the Materials and Process Simulation Center were provided by ARO-DURIP and ONR-DURIP.

REFERENCES

- (1) Tallon, J. L.; Bernhard, C.; Shaked, H.; Hitterman, R. L.; Jorgensen, J. D. Generic Superconducting Phase Behavior in High- T_c Cuprates: T_c Variation with Hole Concentration in $\text{YBa}_2\text{Cu}_3\text{O}_{7-\delta}$. *Phys. Rev. B* **1995**, *51*, 12911–12914.

- (2) Obertelli, S. D.; Cooper, J. R.; Tallon, J. L. Systematics in the Thermoelectric Power of High- T_c Oxides. *Phys. Rev. B* **1992**, *46*, 14928–14931.
- (3) Newns, D. M.; Tsuei, C. C.; Huebener, R. P.; van Bentum, P. J. M.; Pattnaik, P. C.; Chi, C. C. Quasiclassical Transport at a van Hove Singularity in Cuprate Superconductors. *Phys. Rev. Lett.* **1994**, *73*, 1695–1698.
- (4) Kontani, H. Theory of Thermoelectric Power in High- T_c Superconductors. *J. Phys. Soc. Jpn.* **2001**, *70*, 2840–2843.
- (5) Trodahl, H. J. Thermopower of the Superconducting Cuprates. *Phys. Rev. B* **1995**, *51*, 6175–6178.
- (6) J. Rossat-Mignod, J.; Regnault, L. P.; Vettier, C.; Bourges, P.; Burlet, P.; Bossy, J.; Henry, J. Y.; Lapertot, G. Neutron Scattering Study of the $\text{YBa}_2\text{Cu}_3\text{O}_{6+x}$ System. *Phys. C* **1991**, *185*, 86–92.
- (7) Mook, H. A.; Yethiraj, M.; Aeppli, G.; Mason, T. E.; Armstrong, T. Polarized Neutron Determination of the Magnetic Excitations in $\text{YBa}_2\text{Cu}_3\text{O}_7$. *Phys. Rev. Lett.* **1993**, *70*, 3490–3493.
- (8) Bourges, P.; Fong, H. F.; Regnault, L. P.; Bossy, J.; Vettier, C.; Milius, D. L.; Aksay, I. A.; Keimer, B. High-Energy Spin Excitations in $\text{YBa}_2\text{Cu}_3\text{O}_{6.5}$. *Phys. Rev. B* **1997**, *56*, R11439–R11442.
- (9) Fong, H. F.; Bourges, P.; Sidis, Y.; Regnault, L. P.; Ivanov, A.; Gu, G. D.; Koshizuka, N.; Keimer, B. Neutron Scattering from Magnetic Excitations in $\text{Bi}_2\text{Sr}_2\text{CaCu}_2\text{O}_{8+\delta}$. *Nature* **1999**, *398*, 588–591.
- (10) Fong, H. F.; Bourges, P.; Sidis, Y.; Regnault, L. P.; Bossy, J.; Ivanov, A.; Milius, D. L.; Aksay, I. A.; Keimer, B. Spin Susceptibility in Underdoped $\text{YBa}_2\text{Cu}_3\text{O}_{6+x}$. *Phys. Rev. B* **2000**, *61*, 14773–14786.
- (11) Fong, H. F.; Keimer, B.; Reznik, D.; Milius, D. L.; Aksay, I. A. Polarized and Unpolarized Neutron-Scattering Study of the Dynamical Spin Susceptibility of $\text{YBa}_2\text{Cu}_3\text{O}_7$. *Phys. Rev. B* **1996**, *54*, 6708–6720.
- (12) Fong, H. F.; Keimer, B.; Anderson, P. W.; Reznik, D.; Doğan, F.; Aksay, I. A. Phonon and Magnetic Neutron Scattering at 41 meV in $\text{YBa}_2\text{Cu}_3\text{O}_7$. *Phys. Rev. Lett.* **1995**, *75*, 316–319.
- (13) He, H.; Bourges, P.; Sidis, Y.; Ulrich, C.; Regnault, L. P.; Pailhès, S.; Berzigiarova, N. S.; Kolesnikov, N. N.; Keimer, B. Magnetic Resonant Mode in the Single-Layer High-Temperature Superconductor $\text{Tl}_2\text{Ba}_2\text{CuO}_{6+\delta}$. *Science* **2002**, *295*, 1045–1047.
- (14) He, H.; Sidis, Y.; Bourges, P.; Gu, G. D.; Ivanov, A.; Koshizuka, N.; Liang, B.; Lin, C. T.; Regnault, L. P.; Schoenherr, E.; Keimer, B. Resonant Spin Excitation in an Overdoped High Temperature Superconductor. *Phys. Rev. Lett.* **2001**, *86*, 1610–1613.
- (15) Fauqué, B.; Sidis, Y.; Campogna, L.; Ivanov, A.; Hradil, K.; Ulrich, C.; Rykov, A. I.; Keimer, B.; Bourges, P. Dispersion of the Odd Magnetic Resonant Mode in Near-Optimally Doped $\text{Bi}_2\text{Sr}_2\text{CaCu}_2\text{O}_{8+\delta}$. *Phys. Rev. B* **2007**, *76*, 214512.
- (16) Morr, D. K.; Pines, D. The Resonance Peak in Cuprate Superconductors. *Phys. Rev. Lett.* **1998**, *81*, 1086–1089.
- (17) Emery, V. J.; Kivelson, S. A.; Zachar, O. Spin-gap Proximity Effect Mechanism of High-Temperature Superconductivity. *Phys. Rev. B* **1997**, *56*, 6120–6147.
- (18) Tranquada, J. M.; Woo, H.; Perring, T. G.; Goka, H.; Gu, G. D.; Xu, G.; Fujita, M.; Yamada, K. Quantum Magnetic Excitations from Stripes in Copper Oxide High Temperature Superconductors. *Nature* **2004**, *429*, 534–538.
- (19) Bulut, N.; Scalapino, D. J. Neutron Scattering from a Collective Spin Fluctuation Mode in a CuO_2 Bilayer. *Phys. Rev. B* **1996**, *53*, 5149–5152.
- (20) Liu, D. Z.; Zha, Y.; Levin, K. Theory of Neutron Scattering in the Normal and Superconducting States of $\text{YBa}_2\text{Cu}_3\text{O}_{6+x}$. *Phys. Rev. Lett.* **1995**, *75*, 4130–4133.
- (21) Eschrig, M. The Effect of Collective Spin-1 Excitations on Electronic Spectra in High- T_c Superconductors. *Adv. Phys.* **2006**, *55*, 47–183.
- (22) Sega, I.; Prelovšek, P.; Bonča, J. Magnetic Fluctuations and Resonant Peak in Cuprates: Towards a Microscopic Theory. *Phys. Rev. B* **2003**, *68*, 054524.
- (23) Wise, W. D.; Boyer, M. C.; Chatterjee, K.; Kondo, T.; Takeuchi, T.; Ikuta, H.; Wang, Y.; Hudson, E. W. Charge-Density-Wave Origin of Cuprate Checkerboard Visualized by Scanning Tunneling Microscopy. *Nat. Phys.* **2008**, *4*, 696–699.
- (24) Wise, W. D.; Chatterjee, K.; Boyer, M. C.; Kondo, T.; Takeuchi, T.; Ikuta, H.; Xu, Z.; Wen, J.; Gu, G. D.; Wang, Y.; et al. Imaging Nanoscale Fermi-Surface Variations in an Inhomogeneous Superconductor. *Nat. Phys.* **2009**, *5*, 213–216.
- (25) Capogna, L.; Fauqué, B.; Sidis, Y.; Ulrich, C.; Bourges, P.; Pailhès, S.; Ivanov, A.; Tallon, J. L.; Liang, B.; Lin, C. T.; et al. Odd and Even Magnetic Resonant Modes in Highly Overdoped $\text{Bi}_2\text{Sr}_2\text{CaCu}_2\text{O}_{8+\delta}$. *Phys. Rev. B* **2007**, *75*, 060502.
- (26) Pailhès, S.; Ulrich, C.; Fauqué, B.; Hinkov, V.; Sidis, Y.; Ivanov, A.; Lin, C. T.; Keimer, B.; Bourges, P. Doping Dependence of Bilayer Resonant Spin Excitations in $(\text{Y,Ca})\text{Ba}_2\text{Cu}_3\text{O}_{6+x}$. *Phys. Rev. Lett.* **2006**, *96*, 257001.
- (27) Tranquada, J. M. Neutron Scattering Studies of Antiferromagnetic Correlations in Cuprates. *Handbook of High-Temperature Superconductivity*; Schrieffer, J. R., Brooks, J. S., Eds.; Springer: New York, 2007; pp 257–298.
- (28) Dahm, T.; Hinkov, V.; Borisenko, S. V.; Kordyuk, A. A.; Zabolotnyy, V. B.; Fink, J.; Büchner, B.; Scalapino, D. J.; Hanke, W.; Keimer, B. Strength of the Spin-Fluctuation-Mediated Pairing Interaction in a High-Temperature Superconductor. *Nat. Phys.* **2009**, *5*, 217–221.
- (29) Vignolle, B.; Hayden, S. M.; McMorro, D. F.; Rønnow, H. M.; Lake, B.; Frost, C. D.; Perring, T. G. Two Energy Scales in the Spin Excitations of the High-Temperature Superconductor $\text{La}_{2-x}\text{Sr}_x\text{CuO}_4$. *Nat. Phys.* **2007**, *3*, 163–167.
- (30) Lipscombe, O. J.; Hayden, S. M.; Vignolle, B.; McMorro, D. F.; Perring, T. G. Persistence of High-Frequency Spin Fluctuations in Overdoped Superconducting $\text{La}_{2-x}\text{Sr}_x\text{CuO}_4$ ($x = 0.22$). *Phys. Rev. Lett.* **2007**, *99*, 067002.
- (31) Paramekanti, A.; Randeria, M.; Trivedi, N. Projected Wave Functions and High Temperature Superconductivity. *Phys. Rev. Lett.* **2001**, *87*, 217002.
- (32) Kamimura, H.; Hamada, T.; Matsuno, S.; Ushio, H. A Novel Approach to the Polaronic Metallic State of Cuprate Superconductors and the d-Wave Pairing Mechanism. *J. Supercond.* **2002**, *15*, 379–385.
- (33) Bersuker, I. B. *The Jahn–Teller Effect*; Cambridge University Press: Cambridge, U.K., 2006.
- (34) Yao, D. X.; Carlson, E. W.; Campbell, D. K. Magnetic Excitations of Stripes Near a Quantum Critical Point. *Phys. Rev. Lett.* **2006**, *97*, 017003.
- (35) Koizumi, H. Spin-Wave Excitations in Effectively Half-Filled Mott Insulators. *J. Phys. Soc. Jpn.* **2008**, *77*, 104704.
- (36) Perry, J. K.; Tahir-Kheli, J.; Goddard, W. A. Antiferromagnetic Band Structure of La_2CuO_4 : Becke-3–Lee–Yang–Parr Calculations. *Phys. Rev. B* **2001**, *63*, 144510.
- (37) Perry, J. K.; Tahir-Kheli, J.; Goddard, W. A. Ab Initio Evidence for the Formation of Impurity $d_{3z^2-r^2}$ Holes in Doped $\text{La}_{2-x}\text{Sr}_x\text{CuO}_4$. *Phys. Rev. B* **2002**, *65*, 144501.
- (38) Tahir-Kheli, J.; Goddard, W. A. Chiral Plaquette Polaron Theory of Cuprate Superconductivity. *Phys. Rev. B* **2007**, *76*, 014514.
- (39) Tahir-Kheli, J.; Goddard, W. A. The Chiral Plaquette Polaron Paradigm (CPPP) for High Temperature Cuprate Superconductors. *Chem. Phys. Lett.* **2009**, *472*, 153–165. The acronym

CPPP was used rather than CPP (chiral plaquette pairing) that is used here.

- (40) Aeppli, G.; Hayden, S. M.; Mook, H. A.; Fisk, Z.; Cheong, S.-W.; Rytz, D.; Remeika, J. P.; Espinosa, G. P.; Cooper, A. S. Magnetic Dynamics of La_2CuO_4 and $\text{La}_{2-x}\text{Ba}_x\text{CuO}_4$. *Phys. Rev. Lett.* **1989**, *62*, 2052–2055.
- (41) Sulewski, P. E.; Fleury, P. A.; Lyons, K. B.; Cheong, S.-W.; Fisk, Z. Light Scattering from Quantum Spin Fluctuations in R_2CuO_4 (R = La, Nd, Sm). *Phys. Rev. B* **1990**, *41*, 225–230.
- (42) Newman, M. E. J.; Ziff, R. M. Fast Monte Carlo Algorithm for Site or Bond Percolation. *Phys. Rev. E* **2001**, *64*, 016706.
- (43) Takami, T.; Zhou, J.-S.; Cheng, J.-G.; Goodenough, J. B.; Matsubayashi, K.; Uwatoko, Y. Study of the Onset of Superconductivity in Underdoped $\text{La}_{2-x}\text{Sr}_x\text{CuO}_4$. *New J. Phys.* **2009**, *11*, 013057.
- (44) Emery, V. J.; Kivelson, S. A. Importance of Phase Fluctuations in Superconductors with Small Superfluid Density. *Nature* **1995**, *374*, 434–437.
- (45) Manousakis, E. The Spin-1/2 Heisenberg Antiferromagnet on a Square Lattice and its Application to the Cuprous Oxides. *Rev. Mod. Phys.* **1991**, *63*, 1–62.
- (46) Kordyuk, A. A.; Borisenko, S. V.; Knupfer, M.; Fink, J. Measuring the Gap in Angle-Resolved Photoemission Experiments on Cuprates. *Phys. Rev. B* **2003**, *67*, 064504.
- (47) Fischer, Ø.; Kugler, M.; Maggio-Aprile, I.; Berthod, C.; Renner, C. Scanning Tunneling Spectroscopy of High-Temperature Superconductors. *Rev. Mod. Phys.* **2007**, *79*, 353–419.
- (48) Renner, C.; Revaz, B.; Genoud, J.-Y.; Kadowaki, K.; Fischer, Ø. Pseudogap Precursor of the Superconducting Gap in Under- and Overdoped in $\text{Bi}_2\text{Sr}_2\text{CaCu}_2\text{O}_{8+\delta}$. *Phys. Rev. Lett.* **1998**, *80*, 149–152.
- (49) Maggio-Aprile, I.; Renner, C.; Erb, A.; Walker, E.; Fischer, Ø. Direct Vortex Lattice Imaging and Tunneling Spectroscopy of Flux Lines on $\text{YBa}_2\text{Cu}_3\text{O}_{7-\delta}$. *Phys. Rev. Lett.* **1995**, *75*, 2754–2757.
- (50) MacDonald, D. K. *Thermoelectricity: An Introduction to the Principles*; Wiley: New York, 1962.
- (51) Ziman, J. M. *Principles of the Theory of Solids*, 2nd ed.; Cambridge University Press: Cambridge, U.K., 1972.
- (52) Herring, C. Theory of the Thermoelectric Power of Semiconductors. *Phys. Rev.* **1954**, *96*, 1163–1187.